doi:10.1016/j.jmb.2004.02.052 J. Mol. Biol. (2004) 338, 341–352

JMB

Available online at www.sciencedirect.com

SCIENCE DIRECT®

ELSEVIER

High Resolution Crystal Structures of HIV-1 Protease with a Potent Non-peptide Inhibitor (UIC-94017) Active Against Multi-drug-resistant Clinical Strains

Yunfeng Tie[1]†, Peter I. Boross[2,3]†, Yuan-Fang Wang[2] Laquasha Gaddis[2], Azhar K. Hussain[4], Sofiya Leshchenko[4] Arun K. Ghosh[4], John M. Louis[5], Robert W. Harrison[2,6] and Irene T. Weber[1,2]*

[1]*Department of Chemistry Georgia State University Atlanta, GA 30303, USA*

[2]*Department of Biology Georgia State University 24 Peachtree Ctr Avenue Atlanta, GA 30303, USA*

[3]*Department of Biochemistry and Molecular Biology, Faculty of Medicine, University of Debrecen, Debrecen, Hungary*

[4]*Department of Chemistry University of Illinois at Chicago Chicago, IL 60607, USA*

[5]*Laboratory of Chemical Physics, National Institute of Diabetes and Digestive and Kidney Diseases, The National Institutes of Health, Bethesda MD 20892, USA*

[6]*Department of Computer Science, Georgia State University, Atlanta GA 30303, USA*

**Corresponding author*

The compound UIC-94017 (TMC-114) is a second-generation HIV protease inhibitor with improved pharmacokinetics that is chemically related to the clinical inhibitor amprenavir. UIC-94017 is a broad-spectrum potent inhibitor active against HIV-1 clinical isolates with minimal cytotoxicity. We have determined the high-resolution crystal structures of UIC-94017 in complexes with wild-type HIV-1 protease (PR) and mutant proteases PR_{V82A} and PR_{I84V} that are common in drug-resistant HIV. The structures were refined at resolutions of 1.10–1.53 Å. The crystal structures of PR and PR_{I84V} with UIC-94017 ternary complexes show that the inhibitor binds to the protease in two overlapping positions, while the PR_{V82A} complex had one ordered inhibitor. In all three structures, UIC-94017 forms hydrogen bonds with the conserved main-chain atoms of Asp29 and Asp30 of the protease. These interactions are proposed to be critical for the potency of this compound against HIV isolates that are resistant to multiple protease inhibitors. Other small differences were observed in the interactions of the mutants with UIC-94017 as compared to PR. PR_{V82A} showed differences in the position of the main-chain atoms of residue 82 compared to PR structure that better accommodated the inhibitor. Finally, the 1.10 Å resolution structure of PR_{V82A} with UIC-94017 showed an unusual distribution of electron density for the catalytic aspartate residues, which is discussed in relation to the reaction mechanism.

Keywords: HIV protease; crystal structure; drug resistance; catalysis

Introduction

Inhibitors of the HIV-1 protease (PR) are effective antiviral drugs and have dramatically improved the survival of patients infected with HIV-1. However, the long-term therapeutic efficacy is compromised by the rapid selection of drug-resistant variants of the PR.[1] Cross-resistance and multi-drug resistance have been reported in AIDS patients on combination therapy.[2,3] The clinical inhibitors select for different mutations, and complex patterns of mutations have been observed.[4] HIV PR is catalytically active as a dimer, and the catalytic Asp25 residues from both subunits interact closely at the subunit interface. The substrate-binding site consists of subsites S3 to S4′ for peptide substrates extending from residues P3 to

† Y.T. and P.I.B. contributed equally to this work.

Abbreviations used: PR, wild-type HIV-1 protease; PR_{V82A}, PR with V82A mutation; PR_{I84V}, PR with I84V mutation; DMSO, dimethylsulfoxide.

E-mail address of the corresponding author: iweber@gsu.edu

P4′. The clinical inhibitors are observed to bind in PR subsites S2–S2′. Mutations that alter the inhibitor-binding site are common, including mutations of residues D30, M46, I50, V82 and I84. Other mutations alter residues located far from the inhibitor-binding site, such as L90M. Mutants with either increased or decreased catalytic activity, inhibition or stability relative to the wild-type enzyme have been observed.[5–9] Crystal structures of resistant mutants have provided the molecular basis for the altered enzymatic properties and the resistant phenotype.[7,10–12] The result of detailed structural and kinetic studies is that individual mutations, and the tested pairs of mutations, show a range of effects that depend on the specific combination of mutant with substrate or inhibitor. Therefore, it is important to obtain high-resolution crystal structures in order to observe the small structural changes associated with the mutations.

Novel inhibitors that target critical conserved regions of the PR different from those of the current drugs are expected to be more active against resistant variants of HIV-1. A novel non-peptide inhibitor UIC-94017 (TMC114) has been developed that is extremely potent *in vivo* against a wide spectrum of HIV strains including multi-drug-resistant clinical strains.[13] This promising non-peptidic inhibitor is in Phase IIB clinical trials. This compound is chemically related to the clinical inhibitor amprenavir, and was designed with a novel *bis*-tetrahydrofuranylurethane (*bis*-THF) group to incorporate additional polar interactions with main-chain atoms of the PR dimer. Crystal structures of complexes of the UIC-94017 with PR and two of the most common drug-resistant mutants, PR_{V82A} and PR_{I84V}, have been determined at high resolution to understand the molecular basis for the potency of this compound.

Results

Chemical synthesis of UIC-94017

The synthesis of UIC-94017 (**1**) is outlined in Figure 1. Commercially available optically active epoxide **3**[14] was reacted with isobutylamine in 2-propanol at 84 °C for six hours. The resulting amino alcohol was reacted with 4-nitrobenzene-sulfonyl chloride to provide the sulfonamide derivative **3**.[15] Reduction of nitro group of **4** by catalytic hydrogenation over 10% Pd–C in ethyl acetate provided the corresponding aromatic amine. Trifluoroacetic acid promoted removal of BOC-group followed by reaction of the resulting diamine with mixed carbonate **5**[16] furnished inhibitor **1**[17] selectively. Synthesis of UIC-94017 was confirmed by ^{1}H-NMR.

Enzyme kinetics and relative inhibition of PR_{V82A} and PR_{I84V}

PR and the drug-resistant mutant proteases, PR_{V82A} and PR_{I84V}, catalyze the hydrolysis of the chromogenic substrate, an analog of the CA-p2 cleavage site in the Gag-Pol polyprotein, between Nle and (NO_2)Phe, and their catalytic activities are competitively inhibited by UIC-94017. Saturation kinetics were observed for PR, PR_{V82A} and PR_{I84V}-catalyzed hydrolysis of substrate. The kinetic parameters are summarized in Table 1. Overall, similar k_{cat}/K_m values were observed: PR_{V82A} and PR_{I84V} showed 85% and 71% of the PR value, respectively. PR_{I84V} showed a fourfold increase in K_m, and a threefold increase in K_i for UIC-94017 as compared to PR and PR_{V82A}. Most of the other clinical inhibitors showed significantly poorer relative inhibition of the protease with V82A or I84V mutations.[18] Amprenavir was an

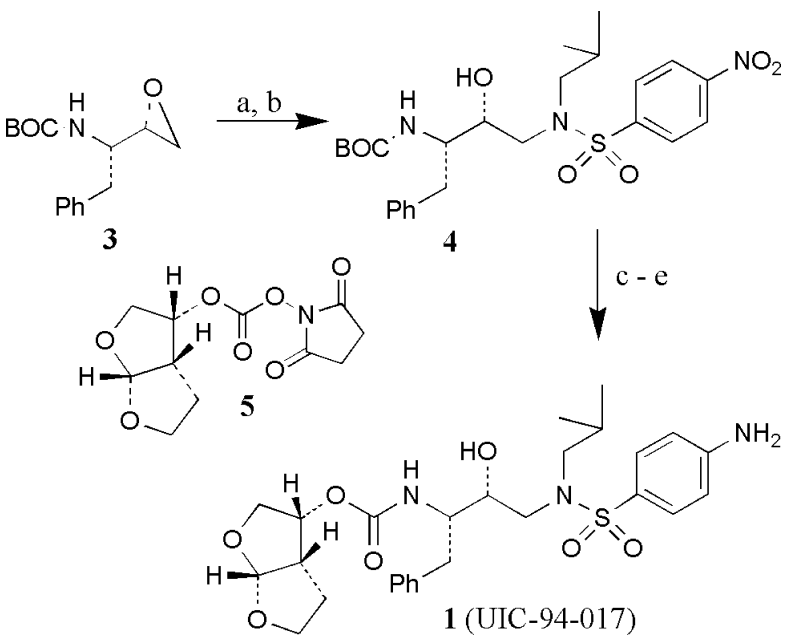

Figure 1. Synthesis of UIC-94017. Reagents and conditions: (a) Me_2-$CHCH_2NH_2$, 2-propanol, 84 °C, six hours; (b) *p*-NO_2-$C_6H_4SO_2Cl$, aq. $NaHCO_3$, CH_2Cl_2; (c) H_2, 10% Pd–C, EtOAc; (d) CF_3CO_2H, CH_2Cl_2; (e) **5**, Et_3N then diamine.

Table 1. Kinetic data

Protease	K_m (μM)	k_{cat} (min^{-1})	k_{cat}/K_m (min^{-1} μM^{-1})	K_i (nM)
PR	55 ± 7	285 ± 9.5	5.18 ± 0.19	1.0 ± 0.2
PR_{V82A}	44 ± 6.5	194.5 ± 7.6	4.42 ± 0.13	1.3 ± 0.2
PR_{I84V}	211 ± 24	780 ± 47	3.7 ± 0.47	3.2 ± 0.7

Kinetic parameters for protease-catalyzed hydrolysis of chromogenic substrate and inhibition constants for the hydrolytic reaction with the inhibitor UIC-94017.

exception showing only two and threefold increased K_i for V82A and I84V mutants, respectively.

Description of the high-resolution crystal structures

The crystal structures of PR and drug-resistant mutants PR_{V82A} and PR_{I84V} have been determined in complex with UIC-94017. Crystallographic statistics are summarized in Table 2. The crystallographic asymmetric units contain a PR dimer with the residues in the two subunits numbered 1–99 and 1′–99′. The three structures were determined in two different space groups and were refined to resolutions of 1.10–1.53 Å and *R*-factors of 0.117–0.134 including solvent molecules, anisotropic *B*-factors and hydrogen atoms. These high-resolution crystal structures showed excellent electron density for all the protease atoms, the inhibitor, and solvent molecules. The electron density map for Tyr59′ and interacting atoms in the PR structure is shown in Figure 2. The average *B*-factors were low for protein and inhibitor atoms. The highest resolution structure of PR_{V82A} had the lowest *R*-factor. PR_{V82A} showed the lowest

Table 2. Crystallographic data statistics

	PR	PR_{V82A}	PR_{I84V}
Space group	$P2_12_12$	$P2_12_12_1$	$P2_12_12$
Unit cell dimensions (Å)			
a	58.26	50.79	58.32
b	85.91	57.87	86.22
c	46.05	61.94	45.85
Resolution range (Å)	50–1.30	50–1.10	50–1.53
Unique reflections	56,890	74,707	35,966
R_{merge} (%) overall (final shell)	6.5 (26.8)	5.2 (19.6)	8.2 (31.2)
Data range for refinement (Å)	10–1.30	10–1.10	10–1.53
R_{work} (%)	13.42	11.74	12.98
R_{free} (%)	17.34	14.53	19.65
No. of solvent (total occupancies)	210	221.6	193
Completeness (%) overall (final shell)	98.6 (90.2)	99.7 (97.6)	99.3 (97.3)
RMS deviation from ideality			
Bonds (Å)	0.014	0.016	0.012
Angle distance (Å)	0.038	0.037	0.035
Average *B*-factors (Å^2)			
Main-chain	14.9	8.0	15.9
Side-chain	19.2	13.1	21.9
Inhibitor	10.8	7.4	14.1
Solvent	31.1	24.1	32.1

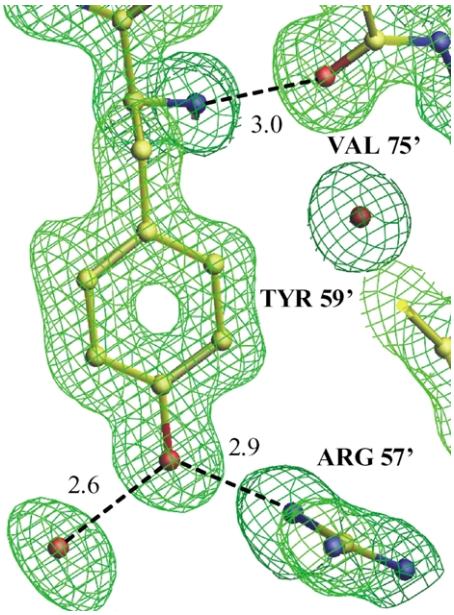

Figure 2. $2F_o - F_c$ electron density map for Tyr59′ of PR complex. The contour level is 1.7σ. Hydrogen bonds are indicated by broken lines with the interatomic distance in Å.

average *B*-factors of 8.0 Å^2 for protein main-chain atoms, compared to values of about 15 Å^2 for the other structures. The inhibitor atoms also had the lowest average *B*-factors for the complex with PR_{V82A}: 7.4 Å^2 compared to 10.8 Å^2 and 14.1 Å^2 for PR and PR_{I84V}, respectively.

Alternate conformations were modeled for residues in all the crystal structures. There were 36 residues with two alternate conformations modeled for PR, 37 for PR_{V82A} and 41 for PR_{I84V} mutant (Table 3). There was clear electron density for the alternate positions of these side-chains, as shown by the examples in Figure 3. The residues with alternate conformations were not the same in both subunits, or in all three structures. However, PR and PR_{I84V} showed a similar pattern, probably because they are in the same space group, and both showed two conformations of the inhibitor. Most alternate conformations were observed for the side-chains of surface residues, especially residues with longer side-chains, such as arginine, lysine, glutamine and glutamic acid. The side-chains of Ile33′, Ile64, Leu89, and Leu97 are in internal hydrophobic regions. The side-chains of seven amino acid residues close to the inhibitor, Arg8, Asp30, Val32, Ile47, Ile50, Pro81, Val82, and Ile84, showed alternate conformations in at least one subunit. Disorder was previously reported for Val32, Val82 and Ile84 in ternary complexes of protease bound to substrate analogs.[11]

The main-chain atoms of Ile50 and 50′ in the two subunits had two alternative conformations, with relative occupancies of 0.6 to 0.4, in the two space group $P2_12_12$ structures. The carbonyl groups in these two residues can flip about 180° and still form the hydrogen bonds between the carbonyl

Table 3. Residues with alternate conformations

Residue	PR	PR_{V82A}	PR_{I84V}
Thr4		A[a]	
Leu5		A[b]	
Trp6		B	
Lys7	AB	A	AB
Arg8	**AB**	**AB**	**AB**
Lys14	AB	AB	AB
Gln18	B	A	B
Lys20		AB	
Glu21	AB	B	AB
Asp30	**AB**	**A**	**AB**
Val32	**B**		**B**
Ile33	B		B
Glu34		B	AB
Glu35		B	B
Met36		B	
Ser37	AB	A	A
Leu38		AB	
Pro39		B	
Gly40		B[b]	
Arg41	A	AB	A
Trp42			B
Lys43	B	AB	AB
Lys45	B		AB
Met46	AB	AB	AB
Ile47		**B**	
Ile50	**A[b]B[a]**		**A[b]B[a]**
Gly51	**A[b]B[b]**		
Lys55	A		AB
Arg57		B	
Gln61		A	AB
Ile63		A	
Ile64		A[a]	
Glu65	AB	AB	AB
Lys70	AB	B	AB
Pro81	**B**		
Val/Ala82	**AB**		**AB**
Ile/Val84	**AB**	**A**	**B**
Leu89			A
Leu97	AB	A	AB

The side-chains have alternate conformations in most cases. A, B indicate the subunit. Residues in inhibitor-binding site are indicated in bold.

[a] Alternate positions for both main-chain and side-chain atoms.

[b] Main-chain atoms have alternate positions.

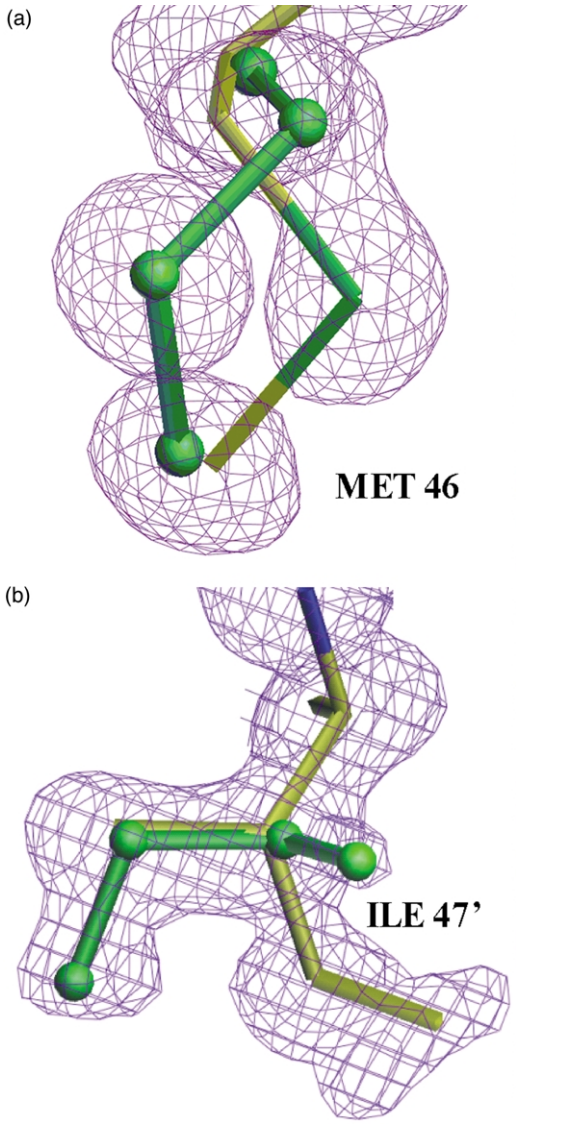

Figure 3. Alternate side-chain positions of PR_{V82A} structure shown in $2F_o - F_c$ map. The $2F_o - F_c$ map was contoured at a level of 1.7σ. The major conformation is colored by atom type, and the minor conformation is in green. (a) Met46, and (b) Ile47′.

oxygen atom and amide nitrogen atom of each residue that link the tips of the flaps. The structure of PR_{V82A} in space group $P2_12_12_1$ showed two alternative conformations of the main-chain atoms between residues 4 and 5, which are located at the dimer surface. Ile64 in PR_{V82A} had alternate main-chain and side-chain conformations in an internal hydrophobic region. The occupancy distribution is 0.7 to 0.3 and there was no change in the interactions with surrounding residues.

Solvent structure in the crystals

Previous crystal structures of HIV protease–inhibitor complexes were modeled with a single shell of solvent molecules.[11] The high quality of diffraction data for the structures described here permitted the modeling of a second shell of solvent. The solvent was modeled with more than 200 water molecules, ions and other small molecules from the crystallization solutions, including many with partial occupancy, depending on the shape of the electron density and the interactions with other molecules. The ions modeled were sodium, chloride, acetate and phosphate. Glycerol and DMSO were fitted to density in the PR and PR_{V82A}. Examples of the electron density maps for solvent regions are shown in Figure 4. The average *B*-factors for the solvent atoms were 24.1 Å^2 for PR_{V82A} and 31–32 Å^2 for PR and PR_{I84V} complexes.

Protease–inhibitor interactions

The crystal structure of HIV-1 PR showed two pseudosymmetric positions of UIC-94017 with

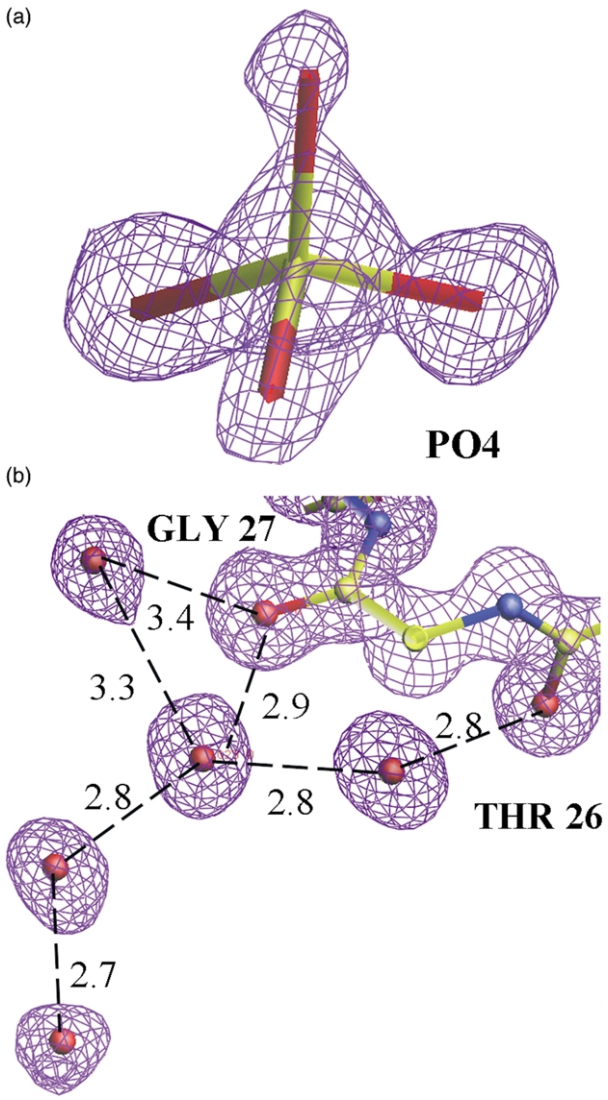

Figure 4. $2F_o - F_c$ electron density maps for solvent molecules of PR_{V82A} structure. The $2F_o - F_c$ map was contoured at a level of 1.7σ. Hydrogen bonds are indicated by broken lines with the interatomic distance in Å. (a) Phosphate, and (b) a set of interacting water molecules.

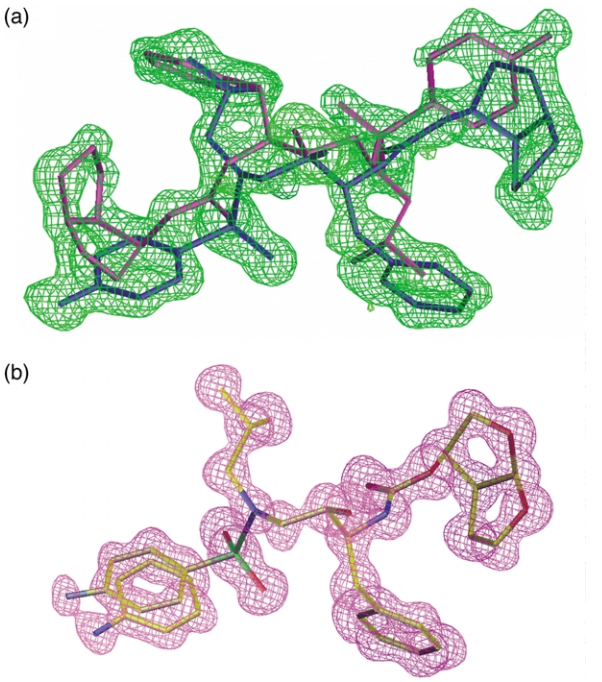

Figure 5. (a) Electron density map of UIC-94017 in PR complex. The $F_o - F_c$ map was contoured at a level of 3.2σ. UIC-94017 is shown in two pseudosymmetric overlapping positions in red and blue bonds. (b) Electron density map of UIC-94017 in PR_{V82A} complex. The $F_o - F_c$ map was contoured at a level of 3.2σ. The map shows one position of UIC-94017 with two conformations for the anilino group.

relative occupancy of 0.55/0.45 (Figure 5(a)). The side-chains of several amino acids in the binding site showed two conformations, as observed previously for hydrophobic side-chains near the peptide analogs.[11] The inhibitor P1 and P1′ groups form van der Waals interactions with protease residues Leu23, Gly49, Ile50, Pro81, Val82, and Ile84 from both subunits. The end groups interact with residues Ala28, Asp29, Asp30, Val32, Ile47 and Ile50. The CG atom of Pro81′ in the PR structure interacts closely with the inhibitor and shows alternate positions with the occupancy distribution of 0.55 to 0.45, which is the same as that of the inhibitor. This suggests that the orientation of the amino acid side-chains correlates with that of the inhibitor. Theoretically, the greater flexibility of the structure will increase the entropy and in turn reduce the interaction energy between protein and inhibitor. The PR–inhibitor hydrogen bond interactions are shown in Figure 6(a). Equivalent interactions exist for both positions of the inhibitor (Table 4). The inhibitor hydroxyl group interacted with all four carboxylate oxygen atoms of the catalytic Asp25 and 25′. The carbonyl oxygen and one of the sulfonamide oxygen atoms forms hydrogen bonds with the water that interacts with the amides of Ile50 and 50′ on the flaps, as observed in most HIV protease–inhibitor complexes.[19] No other water-mediated interactions were observed between PR and UIC-94017. The two oxygen atoms of the *bis*-THF group of the inhibitor are positioned to form hydrogen bond interactions with the main-chain amides of Asp29 and Asp30. The *bis*-THF O28 also formed a close interaction with the OD2 of Asp29, similar to the proton-mediated interaction observed between Asp29 and peptide analogs with P2′ Glu.[11] The amino group at the other end of the inhibitor interacts with the main-chain carbonyl oxygen and the side-chain carboxylate oxygen of Asp30′.

It is instructive to compare the protease interactions of UIC-94017 with those of the structurally related inhibitor, amprenavir. The crystal structure of wild-type protease with amprenavir was determined at 1.9 Å resolution[20] (PDB: 1HPV). Amprenavir had fewer hydrogen bond interactions with the protease residues Asp29 and Asp30

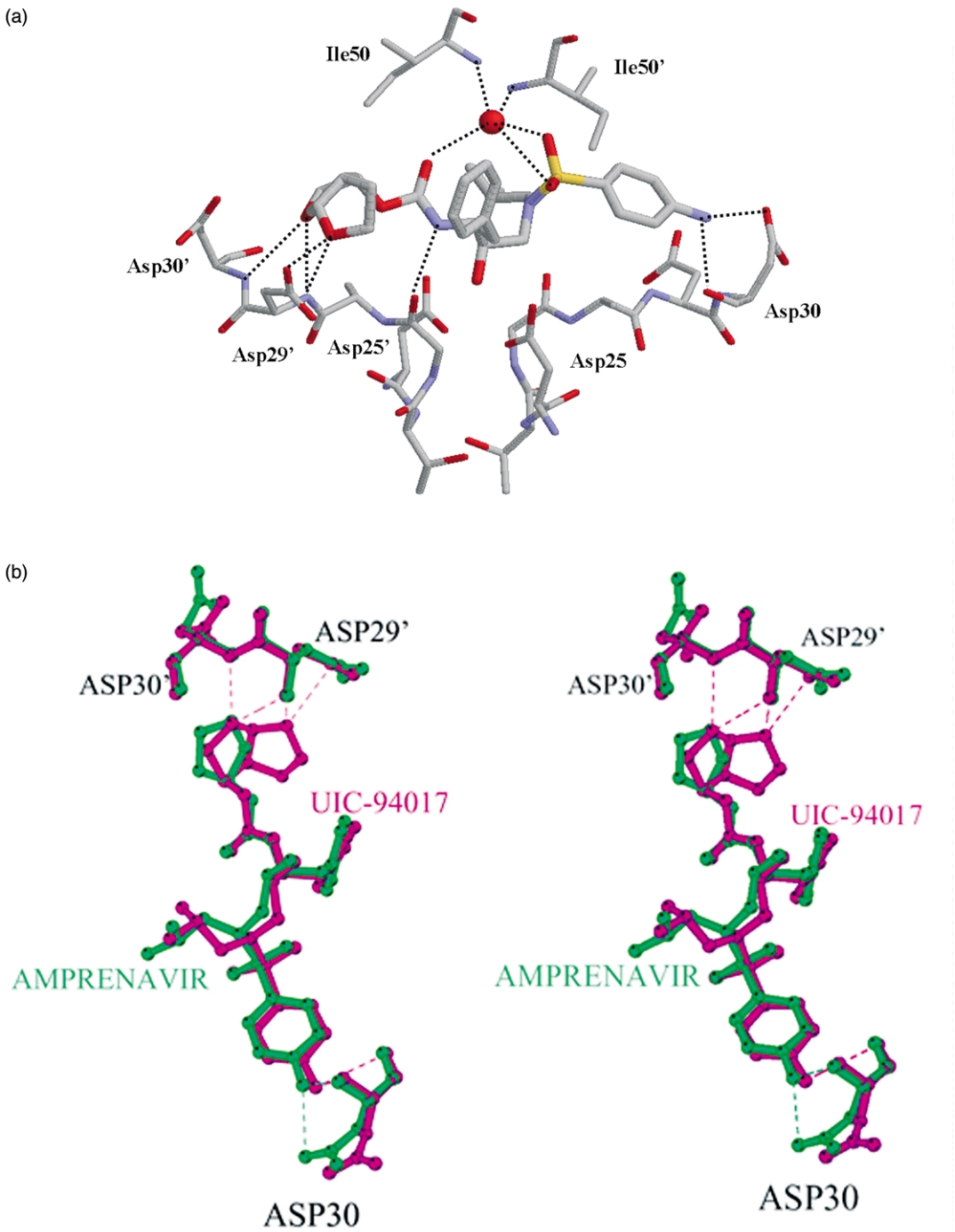

Figure 6. (a) Hydrogen bond interactions of PR with UIC-94017. The PR residues forming hydrogen bond interactions with the major position of UIC-94017 are shown. The interactions of the minor position of UIC-94017 are essentially identical (Table 4). The red sphere indicates a water molecule. Hydrogen bonds are indicated by broken lines. The interactions between OH of UIC-94017 and the carboxylate oxygen atoms of catalytic Asp25 and 25′ are omitted. (b) Major differences in PR interactions with UIC-94017 and amprenavir. The hydrogen bond interactions of PR residues Asp30, Asp29′ and Asp30′ with UIC-94017 and amprenavir are compared in a stereo view. Hydrogen bond interactions are indicated by broken lines. The atoms and interactions in the PR-UIC-94017 structure are green, and the PR-amprenavir atoms and interactions are in red.

(Table 4; Figure 6(b)). Only the amino group of amprenavir formed a hydrogen bond interaction with the carboxylate oxygen of Asp30, while the interactions with the amides of Asp29 and 30 were 3.5 Å long. Amprenavir and UIC-94017 have similar hydrophobic groups with the exception of the *bis*-THF at one end of UIC-94017. Therefore, many of the hydrophobic interactions with PR are similar for both inhibitors. The *bis*-THF group of UIC-94017 introduced one very short van der

Table 4. Protease–inhibitor hydrogen bond interactions

Protease atom	UIC-94017 atom	Distance (Å)			
		WT	V82A	I84V	WT-AMP
Asp25 OD1	OH	**2.7**/2.8	3.0	**2.6**/2.9	2.6
Asp25 OD2	OH	**2.6**/3.1	2.5	**2.4**/3.1	3.1
Asp25′ OD1	OH	**2.8**/2.6	2.5	**2.7**/2.5	2.7
Asp25′ OD2	OH	**3.2**/2.6	3.2	**3.1**/2.5	2.8
Gly**27**′/27 O	NH	**3.2**/3.2	3.1	**3.1**/3.2	(3.6)
Asp**29**′/29 NH	O26	**3.1**/3.0	3.0	**3.1**/3.1	(3.5)
Asp**29**′/29 OD2	O28	**3.2**/3.2	3.3	**3.2**/3.1	
Asp**29**′/29 NH	O28	**3.0**/2.9	2.9	**2.9**/3.0	
Asp**30**/30′ O	NH_2	**3.3**/3.2	(3.5)	**3.2**/3.4	(3.60)
Asp**30**/30′ OD2	NH_2	**2.7**/2.8	**2.8**/2.9[a]	**2.4**/2.6	3.2
Asp**30**′/30 NH	O26	**3.3**/3.3	3.1	**3.3**/(3.5)	(3.5)
H_2OA	O22	**3.0**/3.0	2.8	**2.9**/3.1	3.0
H_2OA	O10═S	**2.4**/2.4	2.8	**2.4**/2.3	2.8
H_2OA	O9═S	**3.3**/3.2		(**3.5**)/3.2	3.4
Ile50 N	H_2OA	2.9	3.0	2.9	2.7
Ile50′ N	H_2OA	2.9	2.9	3.0	2.9
H_2OB	NH_2		2.4		

The protease–UIC-94017 interatomic distances are shown for the crystal structures of PR, PR_{V82A} and PR_{I84V} complexes. The PR and PR_{I84V} complexes have two positions of UIC-94017. The atoms of the major UIC-94017 conformation and interacting PR atoms are indicated in bold. The Asp25 and 25′ carboxylate oxygen atoms interacted with OH in both positions of UIC-94017. PR_{V82A} had one UIC-94017 with two conformations for the anilino group that had different interactions. The interatomic distances are shown for equivalent atoms of amprenavir from 1HPV crystal structure.

[a] The minor conformation of the anilino NH_2 interacted with Asp30 OD2. Two water molecules are indicated as H_2OA and H_2OB. Distances of more than 3.4 Å are in parentheses to indicate that they are too long for good hydrogen bond interactions.

Waals contact of 2.9–3.0 Å with the main-chain carbonyl oxygen of Gly48, which cannot occur in amprenavir. However, both UIC-94017 and amprenavir showed little change in K_i values for PR and mutants V82A and I84V (Table 1).[18]

Comparison of inhibitor interactions in PR and mutants

UIC-94017 has very similar conformation and interactions in all three structures, with the exception of the anilino group, which has two conformations in the PR_{V82A} structure. The crystal structure of PR_{I84V} showed inhibitor bound in two orientations with relative occupancy of 0.69/0.31. The protease–inhibitor interactions are essentially identical with those of PR, except that the lower occupancy inhibitor showed a weak (3.5 Å) interaction with the amide of Asp30 (Table 4). PR_{V82A} showed ordered density for the inhibitor and two conformations for the anilino group as shown in Figure 5(b). The hydrogen bond interactions with UIC-94017 were very similar to those of wild-type enzyme except for those of the amino group (Table 4). The two conformations of the anilino group had relative occupancy of 0.56/0.44. Both conformations of the NH_2 group formed hydrogen bond interactions with the carboxyl oxygen of Asp30, as observed for PR. One conformation also had a weak (3.5 Å) hydrogen bond with the carbonyl oxygen of Asp30, similar to that observed for wild-type enzyme. However, the NH_2 group in the other conformation interacted with a water molecule instead. These small differences suggested that PR_{V82A} had weaker polar interactions with UIC-94017 compared to those of PR.

The PR and mutants had almost identical numbers of van der Waals contacts with inhibitor. The major inhibitor and PR conformations showed 93 van der Waals contacts of less than 4.0 Å, while both the mutants showed 91 contacts. PR_{I84V} mutant showed very similar main-chain structure around the mutated residue compared to the wild-type structure, as shown in Figure 7. Residue I84 in PR shows van der Waals interactions with the inhibitor with interatomic distances of 3.96 Å and 4.38 Å for the two Ile84 side-chain conformations in one subunit, and 5.00 Å in the other subunit. These close van der Waals interactions with inhibitor are lost in PR_{I84V}, consistent with the observed twofold lower inhibition of PR_{I84V} compared to PR. In contrast, PR_{V82A} showed a shift in the position of the main-chain atoms compared to those observed for PR (Figure 7). The shift of 0.50 Å in the 82 α-carbon atom placed the β-carbon atom of Ala82 at 3.76 Å from the closest inhibitor atom, compared to 4.12 Å for the β-carbon of Val82. The other subunit showed a larger shift that positioned the β-carbon atom of Ala82′ at 4.09 Å from inhibitor, compared to 5.18 Å for Val82′. These small shifts result in good van der Waals interactions of Ala82 with inhibitor and offset the loss of the methyl groups of Val82. The structural adaptation of the V82A mutant to accommodate UIC-94017 inhibitor is consistent with the very similar inhibition (K_i) values observed for PR_{V82A} and PR.

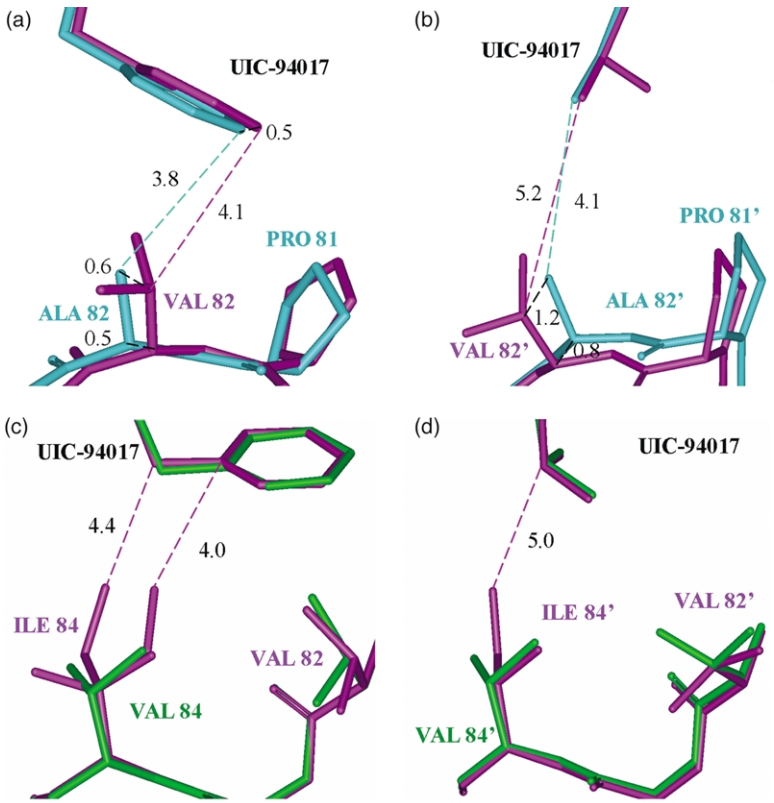

Figure 7. Interactions of mutated residue with UIC-94017 shown in superimposed mutant and PR structures. Only the P1 and P1′ groups of UIC-94017 are shown with the interacting protease residues. Interatomic distances are indicated by broken lines with the separation in Å. PR_{V82A} is shown in blue bonds, PR_{I84V} in green, and PR in red. The major conformation is shown for the side-chains of Val82 and 82′ in PR. The two alternate conformations with similar occupancy are shown for the Ile84 side-chain in PR. (a) PR compared to PR_{V82A} near residue 82. Both Val82 and Ala82 can form van der Waals interactions with UIC-94017. (b) PR compared to PR_{V82A} near residue 82′. Both Val82′ and Ala82′ can form van der Waals interactions with UIC-94017. (c) PR compared to PR_{I84V} near residue 84. Val84 in PR_{I84V} cannot form van der Waals interactions with UIC-94017. (d) PR compared to PR_{I84V} near residue 84′.

Geometry of catalytic aspartate residues and implications for reaction mechanism

The four carboxylate oxygen atoms of Asp25 and 25′ were arranged in almost the same plane and were at distances of 2.52–3.17 Å from the hydroxyl oxygen of UIC-94017 in all the structures (Table 4). Two inner carboxylate oxygen atoms of the two catalytic aspartate residues lie within hydrogen bonding distance of each other in the HIV-1 protease structures (2.59–2.86 Å). Consequently, it has been assumed that one aspartate is protonated and the other has a negative charge. The catalytic aspartate residues have been shown to have different pK_a values of 3.1 and 5.2, consistent with protonation of one catalytic residue.[21] NMR measurements have also indicated that one of the two catalytic aspartate residues was protonated in an HIV-1 protease–inhibitor complex.[22] However, due to the symmetrical arrangement of the catalytic aspartate residues 25 and 25′ in the dimer of HIV protease it has been difficult to determine the location of the expected proton. The existence and location of the proton has implications for the reaction mechanism. Solvent isotope effects were consistent with the reaction proceeding by the rate-limiting step of dissociation of the enzyme-bound amide-hydrate intermediate.[21] Recent kinetic studies using a fluorogenic substrate at pH 6.0 and 1.25 M salt to obtain the solvent isotope effects have also suggested that cleavage of the carbon–nitrogen bond was the major contributor to k_{cat}.[23] The proposed mechanism involves the catalytic aspartate residues together with a water molecule that acts as a nucleophile in attacking the carbonyl carbon of the scissile bond. This mechanism is difficult to support from the crystal structures of HIV protease with transition state analogs, since there is little space for a water molecule next to the catalytic aspartate residues. The closest water molecule cannot interact directly with the catalytic aspartate residues since it lies at the opposite side of the scissile peptide bond next to Ile50 and 50′ of the flaps.

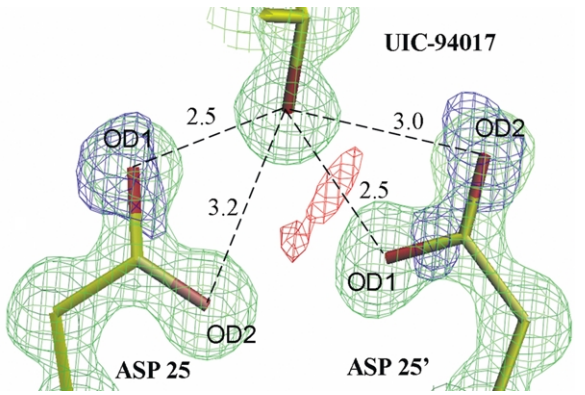

Figure 8. Electron density maps for catalytic aspartate residues of PR_{V82A}. The $2F_o - F_c$ map is green and was contoured at a level of 1.7σ, whereas the $F_o - F_c$ map is contoured at 3.2σ and colored red for positive and blue for negative. Polar interactions are indicated by broken lines with the interatomic distances in Å. The carboxylate oxygen atoms of Asp25 and 25′ are labeled.

The electron density for the catalytic aspartate residues can be examined for details relevant to the reaction mechanism. The crystal structures of PR and PR_{I84V} showed little or no $F_o - F_c$ difference density around the Asp25 and 25′ side-chains, in particular, there is no positive difference density suggesting a proton. These structures were refined at 1.3 Å and 1.5 Å resolution, respectively, and the lower resolution and disordered inhibitor may mask any density for a proton. However, the atomic 1.10 Å resolution of the PR_{V82A} structure and the presence of ordered density for inhibitor revealed differences in the electron density around the catalytic aspartate residues. In fact, significant $F_o - F_c$ difference density was observed for the carboxylate oxygen atoms, in contrast to the other Asp side-chains in the structure (Figure 8). The two outer carboxylate oxygen atoms (OD2) showed negative difference density. A streak of positive density was observed between the hydroxyl group of the inhibitor and the inner and closest OD1 of Asp25′ (2.53 Å separation of OH and OD1), which may indicate a hydrogen atom. This positive density is reduced, but not eliminated, when hydrogen is added to the Asp25′ OD1. The unusual negative difference density can be interpreted as a redistribution of the electrons in the two C–O bonds in the Asp side-chain to a less symmetric arrangement in which the C–O bond furthest from the center has more double bond character, and the other has less. Free atom refinement of the carboxylate groups gave distances of 1.27 Å for both C–O bonds in Asp25, while Asp25′ showed asymmetry with 1.23 Å for C–OD1 and 1.29 Å for C–OD2, consistent with protonation of OD1 (Figure 8). However, the free atom refinement did not significantly change the negative density. Further analysis of the data by charge density analysis or quantum calculations will be necessary to understand the distribution of electrons at the active site. However, the difference densities suggest a more complex mechanism than protonation of a carboxylate oxygen.

Discussion

The UIC-94017 inhibitor is in clinical trials for further development as a new antiviral agent for treatment of primary and multi-PR inhibitor-resistant HIV infections due to its favorable pharmacokinetics.[13] The hydrogen bond interactions of UIC-94017 with HIV PR can be compared to those of substrate analogs. PR recognizes peptide substrates and peptidic inhibitors by means of a series of hydrogen bond interactions with the main-chain atoms of the substrate, as observed for crystal structures of PR in complex with substrate analogs.[19] These interactions span about seven peptide residues lying in PR subsites S3–S4′.[24] The clinical inhibitors lie primarily in subsites S2–S2′ and generally show fewer hydrogen bond interactions. The UIC-94017 inhibitor is shorter than the substrate analogs and forms similar hydrogen bonds to PR main-chain groups, including the conserved Asp29.[25] In addition, new polar interactions are formed with the main-chain amide, carbonyl oxygen and the carboxylate oxygen of Asp29. These interactions resemble those of the P2′ Gln or Glu side-chain of peptide analogs.[11,25] These polar interactions of the *bis*-THF of UIC-94017 were not observed for the most closely related clinical inhibitor, amprenavir. Hence, the UIC-94017 inhibitor more closely mimics many of the natural substrates in the interactions with the PR main-chain atoms than observed for the other clinical inhibitors.

The tight binding of the *bis*-THF group to the main-chain atoms of Asp29 and 30 are expected to be important for the potency of UIC-94017 against multi-drug-resistant HIV.[13] These interactions are maintained in the complexes with PR_{V82A} and PR_{I84V}, although PR_{V82A} had a weaker interaction with the carbonyl oxygen of Asp30. PR_{I84V} showed fewer van der Waals interactions of residue 84 with UIC-94017, consistent with a twofold reduction in inhibition as compared to PR. In contrast, PR_{V82A} showed rearrangements of the main-chain atoms around residues 82 and 82′, which permitted closer interaction of Ala82 and 82′ with UIC-94017, and partly compensated for the fewer side-chain atoms in Ala compared to Val. The structural rearrangements are consistent with similar inhibition observed for both PR_{V82A} and PR. The crystal structure reported for PR_{V82A} with the inhibitor A-77003, also showed rearrangements of the backbone atoms in one subunit,[26] while a recent study described fewer interactions of Ala82 with inhibitors saquinavir and ritonavir compared to those of Val82.[12] UIC-94017 is an effective inhibitor of both the V82A and I84V mutants, which are common in drug-resistant clinical isolates. These new crystal structures of HIV PR mutants with UIC-94017 will provide the framework for the design of new inhibitors that are more effective against resistant HIV. The highest resolution structure of PR_{V82A} mutant provides an intriguing view of the catalytic residues and further analysis will help understand the protonation states of the catalytic aspartate residues and the reaction mechanism.

Materials and Methods

Chemical synthesis of UIC-94017

The synthesis is shown in Figure 1. UIC-94017 (compound **1**) was formed by the reaction of the intermediate compounds (1S)-benzyl-3-[*iso*butyl-(4-nitrobenzenesulfonyl)amino]-(2R)-hydroxy-propyl]-carbamic acid *tert*-butylester (compound **4**) and bis-tetrahydrofuranylsuccinimidyl carbonate (compound **5**). Synthesis of the intermediate compounds is described.

Compound **4** was prepared by heating a stirred solution of *tert*-butyl[S-(R,R)]-(−)-(1-oxiranyl-2-phenylethyl)-carbamate **3** (100 mg, 0.38 mmol) and *iso*butylamine (0.23 ml, 2.28 mmol) in *iso*propanol (3 ml) under reflux

for six hours. Evaporation of solvent under reduced pressure gave a residue, which was chromatographed over silica gel (7% MeOH in $CHCl_3$ as the eluent; R_f = 0.35, 10% MeOH in $CHCl_3$) to yield the corresponding amine (126 mg, 99%).

4-Nitrobenzenesulfonyl chloride (90 mg, 0.41 mmol) and saturated aqueous sodium bicarbonate (5 ml) were added to a stirred solution of the above amino alcohol (92 mg, 0.27 mmol) in dichloromethane (5 ml). The resulting mixture was stirred at 23 °C for 12 hours, extracted with CH_2Cl_2 and dried over anhydrous Na_2SO_4. Removal of solvent under reduced pressure gave a residue, which was chromatographed over silica gel (3% EtOAc in $CHCl_3$ as the eluent; $R_f = 0.49$, 10% EtOAc in $CHCl_3$) to afford the compound **4** (140 mg, 96%) as a white solid (m.p. 167–169 °C).

Compound **5** was prepared by stirring a solution of (3R,3aS,6aR)-3-hydroxyhexahydrofuro[2,3-b]furan (100 mg, 0.77 mmol), *N*,*N*′-disuccinimidyl carbonate (295 mg, 1.15 mmol), and triethylamine (0.2 ml, 1.54 mmol), in distilled acetonitrile (3 ml) at 23 °C for seven hours. Then, the reaction mixture was concentrated under reduced pressure and the residue was diluted with saturated aqueous sodium bicarbonate (4 ml) and extracted with EtOAc (3 × 5 ml). The combined organic extract was dried over anhydrous Na_2SO_4. Evaporation of the solvent under reduced pressure gave a residue, which was chromatographed over silica gel (1% MeOH in $CHCl_3$ as the eluent; R_f = 0.62, 10% MeOH in $CHCl_3$) to yield the title compound **5** (135 mg, 66%) as a white solid (m.p. 122–125 °C).

Finally, UIC-94017 (**1**) was prepared by adding Pd/C (7 mg) to a solution of compound **4** (64 mg, 0.123 mmol) in EtOAc (10 ml) and stirring the mixture at 23 °C under a hydrogen-filled balloon for 11 hours. The reaction mixture was filtered over Celite and the filter cake was washed with EtOAc. Removal of solvent under reduced pressure, followed by column chromatography over silica gel (7% EtOAc in $CHCl_3$ as the eluent; $R_f = 0.16$, 10% EtOAc in $CHCl_3$) afforded the corresponding aromatic amine (61 mg, 95%). A solution of the above amine (33 mg, 0.07 mmol) in a mixture of 30% trifluoroacetic acid in CH_2Cl_2 (6 ml) was stirred at 23 °C for 40 minutes. After this period, solvent was removed under reduced pressure and the residue was dissolved in CH_2Cl_2 (6 ml). Succinimidyl carbonate **5** (20 mg, 0.07 mmol) and triethylamine (0.1 ml, 0.67 mmol) were added to this solution, and the resulting mixture was stirred for three hours. Removal of solvent under reduced pressure gave a residue, which was chromatographed over silica gel (2% MeOH in $CHCl_3$ as the eluent, $R_f = 0.63$, 10% MeOH in $CHCl_3$) to furnish inhibitor **1** (36 mg, 96%) as a white amorphous solid. ^{1}H-NMR (500 MHz, $CDCl_3$) δ 0.81 (d, 3H, J = 6.6 Hz), 0.90 (d, 3H, J = 6.6 Hz), 1.42–1.46 (M, 1H), 1.57–1.65 (m, 1H), 1.79–1.85 (m, 1H), 2.75–2.81 (m, 2H), 2.87–2.98 (m, 3H), 3.05–3.16 (m, 2H), 3.64–3.71 (m, 2H), 3.82–3.88 (m, 3H), 3.92–3.96 (m, 1H), 4.97–5.01 (m, 2H), 5.63 (d, 1H, J = 5.14 Hz), 6.67 (d, 2H, J = 8.6 Hz), 7.18–7.28 (m, 5H), 7.53 (d, 2H, J = 8.6 Hz); ^{13}C-NMR (125.7 MHz, $CDCl_3$) δ 19.92, 20.18, 25.81, 27.29, 29.68, 35.68, 45.35, 53.77, 55.11, 58.90, 69.61, 70.81, 72.84, 73.36, 109.29, 114.12, 125.99, 126.52, 128.50, 129.41, 137.69, 150.75, 155.43.

Protein preparation and determination of the inhibition constants and kinetic parameters

The stabilized HIV-1 protease (PR), which has been optimized for structural and kinetic studies, bears five mutations, Q7K, L33I and L63I to minimize the autoproteolysis of the protease and C67A and C95 to prevent cysteine-thiol oxidation.[11] PR templates with the appropriate oligonucleotide primers were used to introduce the V82A and I84V mutations. All constructs were generated using the Quick-Change Mutagenesis protocol (Stratagene, La Jolla, CA) and verified by DNA sequencing and mass spectrometry. Proteins were prepared using the protocol described.[11] The chromogenic substrate Lys-Ala-Arg-Val-Nle-*p*-nitroPhe-Glu-Ala-Nle-amide (Sigma) was used in a spectroscopic assay. Protease (final concentration of 70–120 nM) was added to 300 μM substrate in 50 mM sodium acetate (pH 5.0), 0.1 M NaCl, 1 mM EDTA, 1 mM β-mercaptoethanol and assayed over ten minutes for the decrease in absorbance at 310 nm on a Hitachi U-2000 spectrophotometer. The absorbances were converted to substrate concentration *via* a calibration curve. Michealis–Menten analysis used 25–400 μM substrate. The Michaelis–Menten curves were fit using SigmaPlot 8.0.2 (SPSS Inc., Chicago, IL). The K_i values were obtained from the IC_{50} values estimated from a dose–response curve with the spectroscopic assay using the equation $K_i = (IC_{50} - [E]/2)/(1 + [S]/K_m)$, where [E] and [S] are the protease and substrate concentrations, respectively.[27]

Crystallographic analysis

UIC-94017 was dissolved in dimethylsulfoxide (DMSO). Crystals were grown by the hanging-drop vapor-diffusion method using 2:1 to 5:1 ratios of inhibitor to protein. Crystals of PR complex grew with a well solution of 30 mM sodium acetate (pH 4.8), 10% (w/v) NaCl, 10% (v/v) glycerol, 10% (v/v) DMSO and 10% dioxane at room temperature. PR_{V82A} crystals grew using a well solution of 50 mM citrate phosphate buffer (pH 5.0), 40% saturated ammonium sulfate, and 7% DMSO. PR_{I84V} crystals were obtained from 30 mM citrate-phosphate buffer (pH 5.0), 8–9% NaCl, and 10% DMSO. The crystals were frozen with a cryoprotectant of 20–30% glycerol. X-ray diffraction data were collected on the SER-CAT beamline at the Advanced Photon Source, Argonne National Laboratory. Data were processed using the HKL 2000.[28] The structures were solved by molecular replacement using AMoRe.[29] The starting models for molecular replacement were chosen as the highest resolution structures in the same space group as the new crystal structure. The starting models were 1FG6 for the PR complex, 1DAZ for PR_{V82A}, and the new PR-UIC-94017 structure was used to solve the PR_{I84V} mutant. The inhibitor structure was generated using AMMP[30] and fitted manually to the electron density map. The structures were refined including anisotropic *B*-factors using SHELX97,[31] and refitted using O 8.0.[32] Structure solution in the $P2_1$ space group was tested for the PR complex, but the two conformations of inhibitor were not resolved, unlike a previous study.[25] Alternate conformations for residues were modeled where observed. The solvent was modeled with more than 200 water molecules and ions or other solvent molecules from crystallization conditions, including many with partial occupancy. The identity of ions and other solvent molecules from the crystallization conditions were deduced from the shape and peak height of the $2F_o - F_c$ electron density, the potential for hydrogen bond interactions, coordination state and interatomic distances. The PR crystal structure was refined with one sodium ion, two chloride ions, two acetate ions, two glycerol

molecules, and 246 water molecules including partial occupancy sites. The PR_{V82A} structure included chloride, six acetate ions, four phosphate groups, one glycerol, one DMSO, and 275 water molecules including partial occupancy sites. The lowest resolution structure of PR_{I84V} was refined with sodium, three chloride molecules, and 355 water molecules including partial occupancy sites. Hydrogen atom positions were included in the last round of refinement using all data. Figures were made using O[32] and MolScript.[33]

Protein Data Bank accession numbers

The coordinates and structure factors have been deposited in the RCSB Protein Data Bank as 1S6G (PR), 1S65 (PR_{V82A}), and 1S6S (PR_{I84V}).

Acknowledgements

This research was supported in part by the National Institutes of Health grants GM62920 (I.T.W. and R.W.H.) and GM53386 (A.G.), Hungarian OTKA F35191, the Georgia Cancer Coalition, and the Georgia Research Alliance. We thank the staff at the SER-CAT beamline at the Advanced Photon Source, Argonne National Laboratory, for assistance during X-ray data collection. Use of the Advanced Photon Source was supported by the US Department of Energy, Basic Energy Sciences, Office of Science, under Contract No. W-31-109-Eng-38.

References

1. Tamalet, C., Pasquier, C., Yahi, N., Colson, P., Poizot-Martin, I., Lepeu, G. *et al.* (2000). Prevalence of drug resistant mutants and virological response to combination therapy in patients with primary HIV-1 infection. *J. Med. Virol.* **61**, 181–186.
2. Shafer, R. W., Winters, M. A., Palmer, S. & Merigan, T. C. (1998). Multiple concurrent reverse transcriptase and protease mutations and multidrug resistance of HIV-1 isolates from heavily treated patients. *Ann. Intern. Med.* **128**, 906–911.
3. Hertogs, K., Bloor, S., Kemp, S. D., Van den Eynde, C., Alcorn, T. M., Pauwels, R. *et al.* (2000). Phenotypic and genotypic analysis of clinical HIV-1 isolates reveals extensive protease inhibitor cross-resistance: a survey of over 6000 samples. *AIDS*, **14**, 1203–1210.
4. Wu, T. D., Schiffer, C. A., Gonzales, M. J., Taylor, J., Kantor, R., Chou, S. *et al.* (2003). Mutation patterns and structural correlates in human immunodeficiency virus type 1 protease following different protease inhibitor treatments. *J. Virol.* **77**, 4836–4847.
5. Ridky, T. W., Kikonyogo, A., Leis, J., Gulnik, S., Copeland, T., Erickson, J. *et al.* (1998). Drug-resistant HIV-1 proteases identify enzyme residues important for substrate selection and catalytic rate. *Biochemistry*, **37**, 13835–13845.
6. Mahalingam, B., Louis, J. M., Reed, C. C., Adomat, J. M., Krouse, J., Wang, Y. F. *et al.* (1999). Structural and kinetic analysis of drug resistant mutants of HIV-1 protease. *Eur. J. Biochem.* **263**, 238–245.
7. Mahalingam, B., Boross, P., Wang, Y. F., Louis, J. M., Fischer, C. C., Tozser, J. *et al.* (2002). Combining mutations in HIV-1 protease to understand mechanisms of resistance. *Proteins: Struct. Funct. Genet.* **48**, 107–116.
8. Dauber, D. S., Ziermann, R., Parkin, N., Maly, D. J., Mahrus, S., Harris, J. L. *et al.* (2002). Altered substrate specificity of drug-resistant human immunodeficiency virus type 1 protease. *J. Virol.* **76**, 1359–1368.
9. Xie, D., Gulnik, S., Gustchina, E., Yu, B., Shao, W., Qoronfleh, W. *et al.* (1999). Drug resistance mutations can effect dimer stability of HIV-1 protease at neutral pH. *Protein Sci.* **8**, 1702–1707.
10. Hong, L., Zhang, X. C., Hartsuck, J. A. & Tang, J. (2000). Crystal structure of an *in vivo* HIV-1 protease mutant in complex with saquinavir: insights into the mechanisms of drug resistance. *Protein Sci.* **9**, 1898–1904.
11. Mahalingam, B., Louis, J. M., Hung, J., Harrison, R. W. & Weber, I. T. (2001). Structural implications of drug resistant mutants of HIV-1 protease: high resolution crystal structures of the mutant protease/substrate analog complexes. *Proteins: Struct. Funct. Genet.* **43**, 455–464.
12. Prabu-Jeyabalan, M., Nalivaika, E. A., King, N. M. & Schiffer, C. A. (2003). Viability of a drug-resistant human immunodeficiency virus type 1 protease variant: structural insights for better antiviral therapy. *J. Virol.* **77**, 1306–1315.
13. Koh, Y., Nakata, H., Maeda, K., Ogata, H., Bilcer, G., Devasamudram, T. *et al.* (2003). A novel bis-tetrahydrofuranylurethane-containing nonpeptidic protease inhibitors (PI) UIC-94017 (TMC114) potent against multi-PI-resistant HIV *in vitro*. *Antimicrob. Agents Chemother.* **47**, 3123–3129.
14. Ghosh, A. K. & Fidanze, S. (1998). Transition-state mimetics for HIV protease inhibitors: stereocontrolled synthesis of hydroxyethylene and hydroxyethylamine isosteres by ester derived titanium enolate syn- and anti-aldol reactions. *J. Org. Chem.* **63**, 6146–6152.
15. Ghosh, A. K., Kincaid, J. F., Cho, W., Walters, D. E., Krishnan, K., Hussain, K. A. *et al.* (1998). Potent HIV protease inhibitors incorporating high sffinity P_2-ligands and (R)-hydroxyethylaminosufonamide isostere. *Bioorg. Med. Chem. Letters*, **8**, 979–982.
16. Ghosh, A. K. & Chen, Y. (1995). Synthesis and optical resolution of high affinity P_2-ligands for HIV-1 protease inhibitors. *Tetrahedron Letters*, **3**, 505–508.
17. Ghosh, A. K., Kincaid, J. F., Walters, D. E., Chen, Y., Chaudhuri, N. C., Thompson, W. J. *et al.* (1996). Nonpeptidal P_2-ligands for HIV protease inhibitors: structure-based design, synthesis and biological evaluations. *J. Med. Chem.* **39**, 3278–3294.
18. Ronald, M., Klabe, L. T., Bacheler, P. J., Ala, S. E. V. & James, L. M. (1998). Resistance to HIV protease inhibitors: a comparison of enzyme inhibition and antiviral potency. *Biochemistry*, **37**, 8735–8742.
19. Gustchina, A., Sansom, C., Prevost, M., Richelle, J., Wodak, S. Y., Wlodawer, A. & Weber, I. T. (1994). Energy calculations and analysis of HIV-1 protease–inhibitor crystal structures. *Protein Eng.* **7**, 309–317.
20. Kim, E. E., Baker, C. T., Dwyer, M. D., Murcko, M. A., Rao, B. G., Tung, R. D. & Navia, M. A. (1995). Crystal structure of HIV-1 protease in complex with VX-478, a potent and orally bioavailable inhibitor of the enzyme. *J. Am. Chem. Soc.* **117**, 1181–1182.
21. Hyland, L. J., Tomaszek, T. A., Jr & Meek, T. D. (1991). Human immunodeficiency virus-1 protease.

2. Use of pH rate studies and solvent kinetic isotope effects to elucidate details of chemical mechanism. *Biochemistry*, **30**, 8454–8463.
22. Wang, Y. X., Freedberg, D. I., Yamazaki, T., Wingfield, P. T., Stahl, S. J., Kaufman, J. D. *et al.* (1996). Solution NMR evidence that the HIV-1 protease catalytic aspartyl groups have different ionization states in the complex formed with the asymmetric drug KNI-272. *Biochemistry*, **35**, 9945–9950.
23. Porter, D. J., Hanlon, M. H. & Furfine, E. S. (2002). HIV-1 protease: characterization of a catalytically competent enzyme–substrate intermediate. *Biochemistry*, **41**, 1302–1307.
24. Louis, J. M., Weber, I. T., Tozser, J., Clore, G. M. & Gronenborn, A. M. (2000). HIV-1 protease: maturation, enzyme specificity, and drug resistance. *Advan. Pharmacol.* **49**, 111–146.
25. Weber, I. T., Wu, J., Adomat, J., Harrison, R. W., Kimmel, A. R., Wondrak, E. M. & Louis, J. M. (1997). Crystallographic analysis of HIV-1 protease with an analog of the conserved CA-p2 substrate: interactions with frequently occurring Glu at P2′ position of substrate. *Eur. J. Biochem.* **249**, 523–530.
26. Baldwin, W. T., Bhat, T. N., Liu, B., Pattabiraman, N. & Erickson, J. W. (1995). Structural basis of drug resistance for the V82A mutant of HIV-1 proteinase. *Nature Struct. Biol.* **2**, 244–249.
27. Maibaum, J. & Rich, D. H. (1988). Inhibition of porcine pepsin by two substrate analogues containing statine: the effect of histidine at the P2 subsite on the inhibition of aspartic proteinases. *J. Med. Chem.* **31**, 625–629.
28. Otwinowski, Z. & Minor, W. (1997). Processing of X-ray diffraction data in oscillation mode. *Methods Enzymol.* **276**, 307–326.
29. Navaza, J. (1994). AMoRe: an automated package for molecular replacement. *Acta Crystallog. sect. D*, **50**, 157–163.
30. Harrison, R. W. (1993). Stiffness and energy conservation in the molecular dynamics: an improved integrator. *J. Comp. Chem.* **14**, 1112–1122.
31. Sheldrick, G. M. & Schneider, T. R. (1997). High resolution refinement. *Methods Enzymol.* **277**, 319–343.
32. Jones, T. A., Zou, J. Y., Cowan, S. W. & Kjeldgaard, M. (1991). Improved methods for building protein models in electron density maps and the location of errors in these models. *Acta. Crystallog. sect. A*, **47**, 110–119.
33. Kraulis, P. J. (1991). MOLSCRIPT: a program to produce both detailed and schematic plots of protein structures. *J. Appl. Crystallog.* **24**, 946–950.

Edited by I. Wilson

(Received 14 October 2003; received in revised form 13 February 2004; accepted 19 February 2004)